

Article

Fermi-Liquid Nonadiabatic Highly Compressed Cesium Iodide Superconductor

Evgueni F. Talantsev 

M.N. Miheev Institute of Metal Physics, Ural Branch, Russian Academy of Sciences, 18, S. Kovalevskoy St., Ekaterinburg 620108, Russia; evgeny.talantsev@imp.uran.ru

Abstract: The experimental discovery that compressed sulfur hydride exhibits superconducting transition temperature of $T_c = 203$ K by Drozdov et al. (*Nature* **2015**, *525*, 73–76) sparked studies of compressed hydrides. This discovery was not a straightforward experimental examination of a theoretically predicted phase, but instead it was a nearly five-decade-long experimental quest for superconductivity in highly compressed matters, varying from pure elements (hydrogen, oxygen, sulfur), hydrides (SiH_4 , AlH_3) to semiconductors and ionic salts. One of these salts was cesium iodide, CsI, which exhibits the transition temperature of $T_c \cong 1.5$ K at $P = 206$ GPa (Eremets et al., *Science* **1998**, *281*, 1333–1335). Detailed first principles calculations (Xu et al., *Phys Rev B* **2009**, *79*, 144110) showed that CsI should exhibit $T_c \sim 0.03$ K ($P = 180$ GPa). In an attempt to understand the nature of this discrepancy between the theory and the experiment, we analyzed the temperature-dependent resistance in compressed CsI and found that this compound is a perfect Fermi liquid metal which exhibits an extremely high ratio of Debye energy to Fermi energy, $\frac{\hbar\omega_D}{k_B T_F} \cong 17$. This implies that direct use of the Migdal–Eliashberg theory of superconductivity to calculate the transition temperature in CsI is incorrect, because the theory is valid for $\frac{\hbar\omega_D}{k_B T_F} \ll 1$. We also showed that CsI falls into the unconventional superconductors band in the Uemura plot.

Keywords: cesium iodide; insulator-metal transition under pressure; nonadiabatic type of superconductors



Citation: Talantsev, E.F. Fermi-Liquid Nonadiabatic Highly Compressed Cesium Iodide Superconductor.

Condens. Matter **2022**, *7*, 65.

[https://doi.org/10.3390/](https://doi.org/10.3390/condmat7040065)

[condmat7040065](https://doi.org/10.3390/condmat7040065)

Academic Editor: Andrea Perali

Received: 22 October 2022

Accepted: 10 November 2022

Published: 11 November 2022

Publisher's Note: MDPI stays neutral with regard to jurisdictional claims in published maps and institutional affiliations.



Copyright: © 2022 by the author. Licensee MDPI, Basel, Switzerland. This article is an open access article distributed under the terms and conditions of the Creative Commons Attribution (CC BY) license (<https://creativecommons.org/licenses/by/4.0/>).

1. Introduction

Since superconducting transition at 203 K was observed in highly compressed sulfur hydride by Drozdov et al. [1], dozens of superconducting hydrogen-based phases have been discovered [2–17] (extended reviews on the current status of the topic can be found elsewhere [18–20]). The report by Drozdov et al. [1] was the triumphant culmination of a nearly five-decade-long journey in the terra incognita of hydrogen-rich compounds [21] and highly compressed matter [22]. On this journey, the superconductors family was significantly extended and the superconducting transition was experimentally observed in many non-superconducting (at ambient conditions) elements/compounds. At the same time, the transition was not observed in materials for which the first principles calculations (FPC) and the Eliashberg theory [23] of the electron–phonon mediated superconductivity predicted a high critical temperature, T_c . We may mention AlH_3 [24,25] as an outstanding case of this class of materials.

However, more often, the superconducting transition was observed, but predicted T_c significantly exceeds the experimental value. The most notable case of this class of materials is compressed SiH_4 for which Feng et al. [26] calculated a Debye temperature of $T_\theta = 3500 - 4000$ K and $T_c \cong 165$ K, while the experiment performed by Eremets et al. [27] showed that $T_c = 7 - 17$ K.

More intriguingly, there are several highly compressed compounds in which experimentally observed T_c significantly exceeds the calculated value. The most famous case of these highly pressurized compounds is sulfur hydride, for which Li et al. [28] initially

predicted $T_c \cong 80$ K. However, Drozdov et al. [1] reported that the experimentally observed transition temperature is significantly higher, $T_c = 203$ K, and the observed value is in excellent agreement with theoretical calculations reported by Duan et al. [29].

Another material from this category is highly compressed CsI, for which detailed first principles calculations performed by Xu et al. [30] predicted $T_c = 0.03$ K at a pressure of $P = 180$ GPa, while the experimental value reported by Eremets et al. [31] is $T_c \cong 1.5$ K (at $P = 206$ GPa).

In this work, we answer the question, why highly compressed CsI exhibits nearly two orders of magnitude higher T_c in comparison with the predicted value by FPC and the Eliashberg theory of electron–phonon mediated superconductivity. Our answer is that highly compressed CsI exhibits an enormous ratio of the Debye temperature, T_θ , to the Fermi temperature, T_F , $\frac{T_\theta}{T_F} \cong 17$, while the Eliashberg theory [23] of the electron–phonon mediated superconductivity is valid for $\frac{T_\theta}{T_F} \ll 1$.

2. Results

2.1. The Electron–Phonon Coupling Constant and the Debye Temperature in CsI at $p = 206$ GPa

Cesium iodide is isoelectronic with the noble gas solid xenon (i.e., Cs^+ and I^- ions in ionic salt have closed xenon-like electronic shells, and the short-range interaction between Cs^+ and I^- ions in uncompressed salt and two Xe atoms in solid xenon is identical). The main difference between Xe and CsI is the very strong Coulomb interaction in cesium iodide in comparison with xenon [32,33]. The strength of the Coulomb interaction decreases on compression, and at $P \cong 110$ GPa CsI is metallized [31,33].

In the theory of the electron–phonon mediated superconductivity [23,34], the phonon spectrum is one of the primary properties that determine the superconducting transition temperature, T_c , and, thus, this is of great interest to determining the main characteristic parameter of this spectrum, i.e., the Debye temperature, T_θ . This value can be deduced from the fit of temperature-dependent resistance, $R(T)$, to the Bloch–Grüneisen (BG) equation [35–40]:

$$R(T) = R_0 + A \times \left(\frac{T}{T_\theta}\right)^5 \times \int_0^{\frac{T_\theta}{T}} \frac{x^5}{(e^x - 1)(1 - e^{-x})} \cdot dx, \quad (1)$$

where R_0 is the residual resistance at $T \rightarrow 0$ K, and the second term describes the electron–phonon scattering, where A and T_θ are free-fitting parameters. Equation (1) was applied to deduce the Debye temperature in many highly compressed superconductors, for instance, in black phosphorus [41], boron [41], sulphur [42,43], lithium [42], ζ -phase of O_2 [42], SnS [37], GeAs [41], SiH_4 [41], H_3S [41,43], D_3S [41,43], LaH_{10} [41,43], $\text{C2}/m\text{-SnH}_{12}$ [44], Th_4H_{15} [45], ThH_9 [45], ThH_{10} [45], YD_6 [45], metallic hydrogen phase-III [45], and $(\text{La}, \text{Nd})\text{H}_{10}$ [46].

The fit of the $R(T)$ curve of compressed CsI ($P \cong 206$ GPa) reported by Eremets et al. [31] in their Figure 3B of [31] to Equation (1) is shown in Figure 1a. The derived Debye temperature is $T_\theta = 339 \pm 1$ K. From this value and the measured $T_c \cong 1.1$ K [31] (see Figure 5 of [31]), one can calculate the electron–phonon coupling constant, λ_{e-ph} , as the root of an advanced McMillan equation [41]:

$$T_c = \left(\frac{1}{1.45}\right) \times T_\theta \times e^{-\left(\frac{1.04(1+\lambda_{e-ph})}{\lambda_{e-ph} - \mu^*(1+0.62\lambda_{e-ph})}\right)} \times f_1 \times f_2^* \quad (2)$$

$$f_1 = \left(1 + \left(\frac{\lambda_{e-ph}}{2.46(1 + 3.8\mu^*)}\right)^{3/2}\right)^{1/3} \quad (3)$$

$$f_2^* = 1 + (0.0241 - 0.0735 \times \mu^*) \times \lambda_{e-ph}^2 \quad (4)$$

where μ^* is the Coulomb pseudopotential; it can be assumed that $\mu^* = 0.13$ [4,18–20]. In the result, $\lambda_{e-ph} = 0.445$ was calculated as a root of Equations (2)–(4). It can be noted that the deduced $\lambda_{e-ph} = 0.445$ is close to $\lambda_{e-ph} = 0.43$ for aluminum [47]. It should also be mentioned that deduced $T_\theta = 339 \pm 1$ K for CsI is not very different from $T_\theta = 394\text{--}428$ K [48,49] for aluminum.

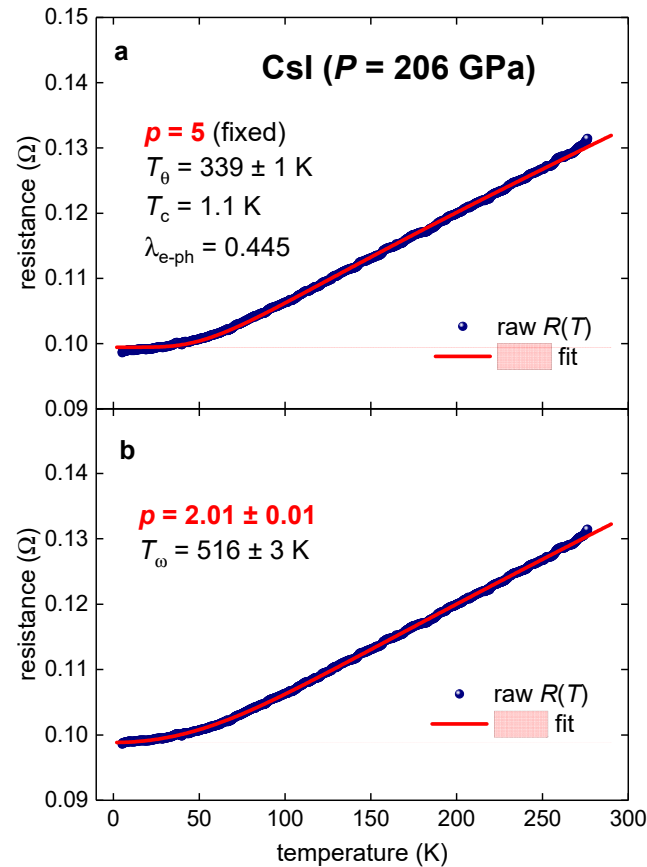


Figure 1. Temperature-dependent resistance data, $R(T)$, in highly compressed cesium iodide ($P = 206$ GPa) and data fits to Equation (1) (panel a) and Equation (5) (panel b). Raw $R(T)$ data are from [31]. (a) $p = 5$, deduced $T_\theta = 339 \pm 1$ K, $R_0 = 0.0995 \Omega$, fit quality R -Squared (COD) = 0.9993; (b) deduced $p = 2.01 \pm 0.01$, $T_\omega = 516 \pm 3$ K, $R_0 = 0.0988 \Omega$, fit quality R -Squared (COD) = 0.9998. 95% confidence bands (in pink) are narrower than the fitting curves width.

One can make a comparison of the $T_\theta = 339$ K and $\lambda_{e-ph} = 0.445$ values derived from experiment ($P = 206$ GPa) with the values computed by first principles calculations [30]. Xu et al. [30] reported $\lambda_{e-ph} = 0.262$ ($P = 180$ GPa) and $\lambda_{e-ph} = 0.257$ ($P = 216$ GPa), and both these values are significantly lower than the one deduced from the experiment here. Xu et al. [30] also calculated the logarithmic phonon frequency $\frac{\hbar}{k_B} \omega_{log} = 285$ K ($P = 180$ GPa), and $\frac{\hbar}{k_B} \omega_{log} = 314$ K ($P = 216$ GPa). By its definition, ω_{log} is close, but does not exactly equal, to the Debye frequency, $T_\theta = \frac{\hbar}{k_B} \omega_D$, and this is what one can see for these values in highly compressed CsI.

By utilizing the Allen–Dynes equation [47,48] and $\mu^* = 0.10$, Xu et al. [30] calculated $T_c = 0.03$ K ($P = 180$ GPa) and $T_c = 0.025$ K ($P = 216$ GPa). Both calculated that the T_c values (and this was acknowledged by the authors of [30]) are by about two orders of magnitude lower than the experimental value. To explain this discrepancy, Xu et al. [30] hypothesized that because first principles calculations show that the CsI exhibits an anisotropic crystalline structure (under pressure), then the Allen–Dynes equation [48,50] (developed for the single-band isotropic superconductors) cannot accurately average an anisotropic case.

Our explanation for the discrepancy is based on a different idea which arose from a more advanced analysis of the temperature-dependent resistance curve described below.

2.2. Perfect Fermi Liquid Conductor CsI at $p = 206$ GPa

Despite the fit of the $R(T)$ curve for the compressed CsI to the BG equation (Equation (1)) having a high quality (Figure 1a), more advanced analysis is based on the approach when the power-law exponent in Equation (1) is a free-fitting parameter [51–55]:

$$R(T) = R_0 + A \times \left(\frac{T}{T_\omega}\right)^p \times \int_0^{\frac{T_\omega}{T}} \frac{x^p}{(e^x - 1)(1 - e^{-x})} \cdot dx. \tag{5}$$

In this approach, the T_ω (Equation (5)) is not any longer the Debye temperature; however, this temperature represents a characteristic energy scalar for the charge carrier interaction in the conductor. There are several integer p -values which associate with a particular charge-carrier interaction mechanism [56–58] and, in particular, $p = 2$ implies that charge carriers in the conductor obey a perfect Landau’s Fermi liquid phenomenology [56–58].

It should be mentioned that for some materials, such as ReBe_{22} [53,59] and $(\text{ScZrNb})_{0.65}[\text{RhPd}]_{0.35}$ [54,60], the power-law exponent is indistinguishable from 5, which implies that these materials are pure electron-phonon-mediated superconductors. However, for the majority of highly compressed superconductors, including the ϵ -Fe phase, the power-law exponent, p , varies between $1.80 \leq p \leq 3.3$ [53–55].

The fit of the $R(T)$ curve in the CsI ($P = 206$ GPa) to Equation (5) is shown in Figure 1b, where it can be seen that the deduced p is indistinguishable from $p = 2.0$. This means that the highly compressed CsI at ($P = 206$ GPa) is a perfect Fermi liquid metal.

2.3. Compressed CsI ($p = 206$ GPa) in the Uemura Plot

One of the widely accepted ways to classify the superconducting state in the material is to position the material in the Uemura plot, i.e., in the plot where the X-axis is the Fermi temperature, T_F , and the Y-axis is the transition temperature, T_c [61,62]. The Fermi temperature in the superconductor can be calculated by the equation [42,63,64]:

$$T_F = \frac{\epsilon_F}{k_B} = \frac{\pi^2}{8 \cdot k_B} \times (1 + \lambda_{e-ph}) \times \xi^2(0) \times \left(\alpha \frac{k_B T_c}{\hbar}\right)^2, \tag{6}$$

where ϵ_F is the Fermi energy, k_B is the Boltzmann constant, $\alpha = \frac{2 \cdot \Delta(0)}{k_B \cdot T_c}$, and $\Delta(0)$ is the amplitude of the ground state energy gap, $\hbar = h/2\pi$ is the reduced Planck constant, and $\xi(0)$ is the ground state coherence length. Based on a very large database on electron-phonon-mediated superconductors [47], one can expect that the CsI ($P = 206$ GPa) which exhibits $\lambda_{e-ph} = 0.445$ should have $\alpha = \frac{2 \cdot \Delta(0)}{k_B \cdot T_c}$ not very different from 3.53, and we used this value in our calculations. Thus, to calculate T_F in the compressed CsI, one needs to estimate the ground state coherence length $\xi(0)$ (Equation (6)).

We deduce $\xi(0)$ for the compressed CsI ($P = 206$ GPa) from the fit of the temperature-dependent upper critical field, $B_{c2}(T)$, to the simplest equation of the Werthamer–Helfand–Hohenberg theory [65,66]:

$$B_{c2}(0) = \frac{\phi_0}{2\pi\xi^2(0)} = -0.697 \times T_c \times \left(\frac{dB_{c2}(T)}{dT}\right)\Bigg|_{T \sim T_c}. \tag{7}$$

The upper critical field represents the applied magnetic field in which the superconducting state collapses in the experiment. We extracted the $B_{c2}(T)$ dataset in highly compressed CsI from the magnetoresistance data reported by Eremets et al. [31] in their Figure 5. To define $B_{c2}(T)$ we utilized a 50% normal state resistance criterion. The fit of the $B_{c2}(T)$ data is shown in Figure 2, from which $\xi(0) = 26 \pm 3$ nm was estimated.

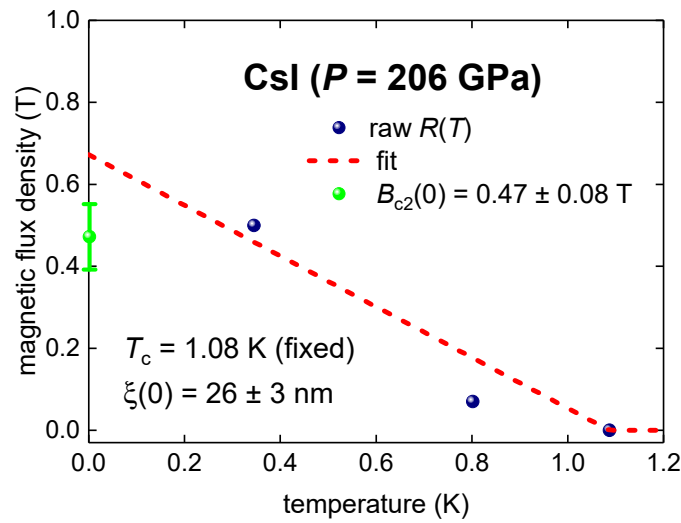


Figure 2. Superconducting upper critical field, $B(T)$, data (blue) for compressed CsI at pressure $p = 206$ GPa (data is from [31]) and fit to WHH model [65,66] (Equation (7)) for which T_c was fixed it is experimental value of 1.087 K; fit quality R -Squared (COD) = 0.90.

From all determined/estimated values, one can calculate $T_F = 20 \pm 4$ K and the ratio of $\frac{T_c}{T_F}$, which varies within a range:

$$0.04 \lesssim \frac{T_c}{T_F} \lesssim 0.07 \tag{8}$$

In the result, the CsI ($P = 206$ GPa) falls into the unconventional superconductors band in the Uemura plot (Figure 3).

It should be noted that the A-15 superconductor V_3Si (which exhibits the electron-phonon-mediated superconductivity with $\lambda_{e-ph} = 0.96$ and $\alpha = \frac{2 \cdot \Delta(0)}{k_B \cdot T_c} = 3.7$ [47,67]) is also located in the unconventional superconductors band in the Uemura plot (Figure 3).

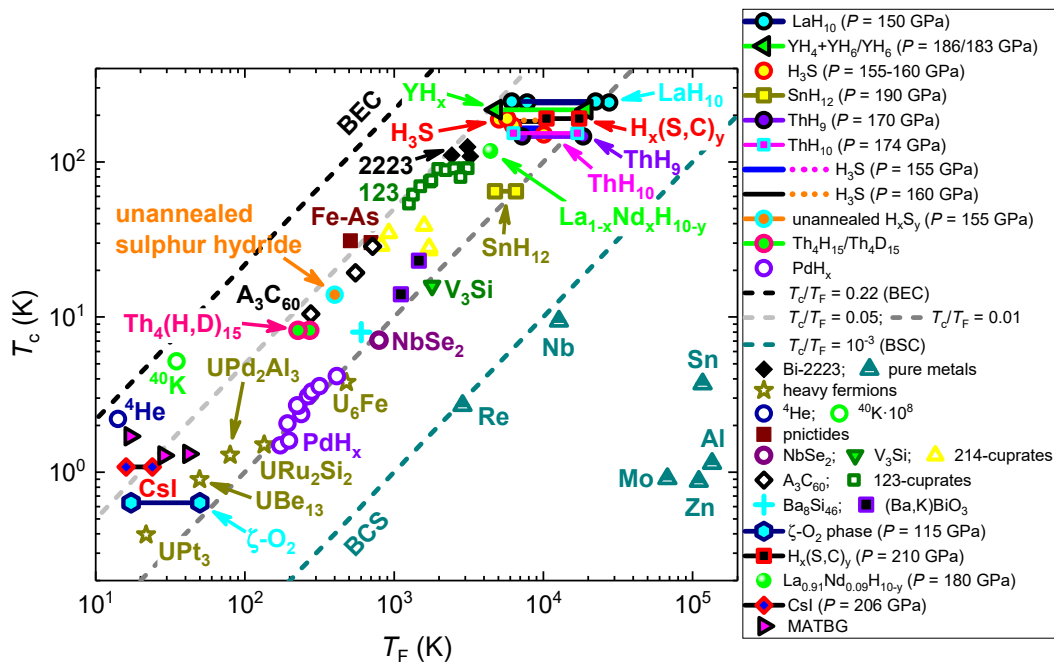


Figure 3. Uemura plot (T_c vs. T_F), where the CsI ($p = 206$ GPa) is shown together with other superconducting families. References on original data (T_c vs. T_F) can be found in [42,44,68,69].

Another material which can be mentioned is the magic-angle twisted bilayer graphene (MATBG) which exhibits very close $T_c = 1.4 \pm 0.3$ K and $T_F = 23 \pm 6$ K values [68,69] (Figure 3) to the compressed CsI.

Thus, our result that the highly compressed CsI (exhibited $\lambda_{e-ph} = 0.445$) falls into the unconventional superconducting band manifests itself as an interesting, but not unique, case. The explanation of this result is based on, roughly speaking, the degree of Cooper pairs overlapping [70]. In CsI and V_3Si , the average size of the Cooper pairs at the low temperature, $\zeta(T \rightarrow 0)$, is comparable with the average distance between pairs and, thus, the pairs overlapping is not significant and is close to the Bose–Einstein condensate [70]. However, in superconductors located on the BCS side of the Uemura plot (Figure 3), the distance between the Cooper pairs centers is significantly smaller than the $\zeta(T \rightarrow 0)$ and the pairs’ overlapping is high. Details for the position of the superfluid 4He in Figure 3 can be found elsewhere [62].

2.4. Nonadiabatic Superconductivity in CsI ($P = 206$ GPa)

It is important to note that one of our central findings is that our analysis shows that the compressed CsI is a remarkably prominent nonadiabatic superconductor. This finding directly follows from the ratio of the Debye temperature, T_θ (for which we used the value deduced from the $R(T)$ data fit to Equation (1), to the Fermi temperature, T_F :

$$\left. \frac{\hbar\omega_D}{k_B T_F} \right|_{CsI, P=206 \text{ GPa}} = \frac{T_\theta = 339 \text{ K}}{T_F = 20 \text{ K}} = 17 \pm 4. \tag{9}$$

Roughly speaking, the Eliashberg theory of electron–phonon-mediated superconductivity [23] is based on Migdal’s theorem [71], which is the many-body version of the principle of Born–Oppenheimer [72]. Namely, it is an argument over adiabaticity, since charge-carrier particles are expected to move faster than ions. Thus, instead of taking the interaction with an electron in a certain position, it is easier to consider the interaction with the full electronic cloud. This consideration is applicable if the electrons are much faster than ions, but in some materials (such as in the C_{60} compound), the Fermi energy and the average phonon energy are just the same, and for these materials the Migdal theorem [71] and the Eliashberg theory [23] are no longer valid.

These kinds of superconductors, designated as nonadiabatic superconductors [73], were first theoretically considered by Pietronero and co-workers nearly three decades ago [73–77]. Pietronero and co-workers [73–77] considered the generalization of the many-body theory of superconductivity in the cases in which the Migdal theorem does not work, typically the systems with very low Fermi energy (or Fermi velocity, or Fermi temperature).

3. Discussion

Equation (9) shows that the compressed CsI ($P = 206$ GPa) exhibits relatively “very fast” phonons and relatively “very slow” charge-carriers. For instance, one can make a comparison of the ratio for the CsI (Equation (9)) with the ratio for elemental electron–phonon superconductors (data for the ratios are taken from [49]):

$$\left. \frac{\hbar\omega_D}{k_B T_F} \right|_{Pb} = \frac{T_\theta = 88 \text{ K}}{T_F = 110000 \text{ K}} = 8 \times 10^{-4}. \tag{10}$$

$$\left. \frac{\hbar\omega_D}{k_B T_F} \right|_{Nb} = \frac{T_\theta = 265 \text{ K}}{T_F = 61800 \text{ K}} = 4 \times 10^{-3}. \tag{11}$$

$$\left. \frac{\hbar\omega_D}{k_B T_F} \right|_{Al} = \frac{T_\theta = 394 \text{ K}}{T_F = 136000 \text{ K}} = 3 \times 10^{-3}. \tag{12}$$

Equation (9) shows that the standard Migdal–Eliashberg theory [23,71] of the electron–phonon-mediated superconductivity is inapplicable for highly compressed CsI and, therefore, this is our explanation for the discrepancy between the superconducting transition

temperature, T_c , predicted by first-principles calculations [30] (following standard Allen–Dynes methodology [48,50]) and the observed T_c in experiment [31].

To the best of our knowledge, such a large $\frac{\hbar\omega_D}{k_B T_F} \Big|_{\text{CsI}, P=206 \text{ GPa}} = 17$ ratio has not been reported for any superconductor to date.

4. Conclusions

In ambient conditions, CsI represents typical ionic salt, which transforms into a metallic state at high pressure. Xu et al. [30] performed first principle calculations for compressed CsI and established that within the Migdal–Eliashberg theory [23,69] this compound should exhibit the superconducting transition temperature $T_c(p = 180 \text{ K}) \sim 0.03 \text{ K}$. Experiments performed by Eremets et al. [31] showed that highly compressed CsI exhibited a nearly two orders of magnitude higher transition temperature $T_c(p = 206 \text{ K}) \sim 1.5 \text{ K}$.

In attempts to find the primary origin for the discrepancy between the theory and the experiment, here we analysed available experimental data measured in highly compressed CsI ($p = 206 \text{ GPa}$) and found that:

1. CsI is a perfect Fermi liquid metal.
2. CsI exhibits an extremely high ratio of Debye energy to Fermi energy, $\frac{\hbar\omega_D}{k_B T_F} \cong 17$. Based on this, one can conclude that the superconducting state in this compound cannot be described by the Migdal–Eliashberg theory [23,69] because the theory is valid when $\frac{\hbar\omega_D}{k_B T_F} \ll 1$.
3. CsI exhibits the ratio of $\frac{T_c=1.1 \text{ K}}{T_F=20 \text{ K}} = 0.055 \pm 0.015$ and, thus, it falls to the unconventional superconductors band in the Uemura plot. This level of the $\frac{T_c}{T_F}$ ratio is typical for many superconductors, including the electron–phonon-mediated A-15 compound V_3Si . It should be mentioned that the magic-angle twisted bilayer graphene exhibits close $T_c = 1.4 \pm 0.3 \text{ K}$ and $T_F = 23 \pm 6 \text{ K}$ values [68,69].

Funding: This research was funded by the Ministry of Science and Higher Education of the Russian Federation, grant number No. AAAA-A18-118020190104-3 (theme “Pressure”).

Data Availability Statement: Not applicable.

Conflicts of Interest: The author declares no conflict of interest. The funders had no role in the design of the study; in the collection, analyses, or interpretation of data; in the writing of the manuscript; or in the decision to publish the results.

References

1. Drozdov, A.P.; Eremets, M.I.; Troyan, I.A.; Ksenofontov, V.; Shylin, S.I. Conventional superconductivity at 203 kelvin at high pressures in the sulfur hydride system. *Nature* **2015**, *525*, 73–76. [[CrossRef](#)] [[PubMed](#)]
2. Drozdov, A.P.; Kong, P.P.; Minkov, V.S.; Besedin, S.P.; Kuzovnikov, M.A.; Mozaffari, S.; Balicas, L.; Balakirev, F.F.; Graf, D.E.; Prakapenka, V.B.; et al. Superconductivity at 250 K in lanthanum hydride under high pressures. *Nature* **2019**, *569*, 528–531. [[CrossRef](#)] [[PubMed](#)]
3. Somayazulu, M.; Ahart, M.; Mishra, A.K.; Geballe, Z.M.; Baldini, M.; Meng, Y.; Struzhkin, V.V.; Hemley, R.J. Evidence for superconductivity above 260 K in lanthanum superhydride at megabar pressures. *Phys. Rev. Lett.* **2019**, *122*, 027001. [[CrossRef](#)] [[PubMed](#)]
4. Semenok, D.V.; Kvashnin, A.G.; Ivanova, A.G.; Svitlyk, V.; Fominski, V.Y.; Sadakov, A.V.; Sobolevskiy, O.A.; Pudalov, V.M.; Troyan, I.A.; Oganov, A.R. Superconductivity at 161 K in thorium hydride ThH_{10} : Synthesis and properties. *Mater. Today* **2020**, *33*, 36–44. [[CrossRef](#)]
5. Chen, W.; Semenok, D.V.; Kvashnin, A.G.; Huang, X.; Kruglov, I.A.; Galasso, M.; Song, H.; Duan, D.; Goncharov, A.F.; Prakapenka, V.B.; et al. Synthesis of molecular metallic barium superhydride: Pseudocubic BaH_{12} . *Nat. Commun.* **2021**, *12*, 273. [[CrossRef](#)]
6. Wang, N.; Shan, P.F.; Chen, K.Y.; Sun, J.P.; Yang, P.T.; Ma, X.L.; Wang, B.S.; Yu, X.H.; Zhang, S.; Chen, G.F.; et al. A low- T_c superconducting modification of Th_4H_{15} synthesized under high pressure. *Supercond. Sci. Technol.* **2021**, *34*, 034006. [[CrossRef](#)]
7. Troyan, I.A.; Semenok, D.V.; Kvashnin, A.G.; Sadakov, A.V.; Sobolevskiy, O.A.; Pudalov, V.M.; Ivanova, A.G.; Prakapenka, V.B.; Greenberg, E.; Gavriliuk, A.G.; et al. Anomalous high-temperature superconductivity in YH_6 . *Adv. Mater.* **2021**, *33*, 2006832. [[CrossRef](#)]

8. Kong, P.; Minkov, V.S.; Kuzovnikov, M.A.; Drozdov, A.P.; Besedin, S.P.; Mozaffari, S.; Balicas, L.; Balakirev, F.F.; Prakapenka, V.B.; Chariton, S.; et al. Superconductivity up to 243 K in yttrium hydrides under high pressure. *Nat. Commun.* **2021**, *12*, 5075. [[CrossRef](#)]
9. Ma, L.; Wang, K.; Xie, Y.; Yang, X.; Wang, Y.; Zhou, M.; Liu, H.; Yu, X.; Zhao, Y.; Wang, H.; et al. High-temperature superconducting phase in clathrate calcium hydride CaH₆ up to 215 K at a pressure of 172 GPa. *Phys. Rev. Lett.* **2022**, *128*, 167001. [[CrossRef](#)]
10. Semenok, D.V.; Troyan, I.A.; Ivanova, A.G.; Kvashnin, A.G.; Kruglov, I.A.; Hanfland, M.; Sadakov, A.V.; Sobolevskiy, O.A.; Pervakov, K.S.; Lyubutin, I.S.; et al. Superconductivity at 253 K in lanthanum–yttrium ternary hydrides. *Mater. Today* **2021**, *48*, 18–28. [[CrossRef](#)]
11. Zhou, D.; Semenok, D.V.; Duan, D.; Xie, H.; Chen, W.; Huang, X.; Li, X.; Liu, B.; Oganov, A.R.; Cui, T. Superconducting praseodymium superhydrides. *Sci. Adv.* **2020**, *6*, eaax6849. [[CrossRef](#)] [[PubMed](#)]
12. Hong, F.; Shan, P.F.; Yang, L.X.; Yue, B.B.; Yang, P.T.; Liua, Z.Y.; Sun, J.P.; Dai, J.H.; Yu, H.; Yin, Y.Y.; et al. Possible superconductivity at ~70 K in tin hydride SnH_x under high pressure. *Mater. Today Phys.* **2022**, *22*, 100596. [[CrossRef](#)]
13. Chen, W.; Semenok, D.V.; Huang, X.; Shu, H.; Li, X.; Duan, D.; Cui, T.; Oganov, A.R. High-temperature superconducting phases in cerium superhydride with a T_c up to 115 K below a pressure of 1 Megabar. *Phys. Rev. Lett.* **2021**, *127*, 117001. [[CrossRef](#)] [[PubMed](#)]
14. Osmond, I.; Moulding, O.; Cross, S.; Muramatsu, T.; Brooks, A.; Lord, O.; Fedotenko, T.; Buhot, J.; Friedemann, S. Clean-limit superconductivity in *Im3m* H₃S synthesized from sulfur and hydrogen donor ammonia borane. *Phys. Rev. B* **2022**, *105*, L220502. [[CrossRef](#)]
15. Semenok, D.V.; Troyan, I.A.; Sadakov, A.V.; Zhou, D.; Galasso, M.; Kvashnin, A.G.; Ivanova, A.G.; Kruglov, I.A.; Bykov, A.A.; Terent'ev, K.Y.; et al. Effect of magnetic impurities on superconductivity in LaH₁₀. *Adv. Mater.* **2022**, *34*, 2204038. [[CrossRef](#)]
16. Bi, J.; Nakamoto, Y.; Zhang, P.; Shimizu, K.; Zou, B.; Liu, H.; Zhou, M.; Liu, G.; Wang, H.; Ma, Y. Giant enhancement of superconducting critical temperature in substitutional alloy (La,Ce)H₉. *Nat. Commun.* **2022**, *13*, 5952. [[CrossRef](#)]
17. Li, Z.; He, X.; Zhang, C.; Wang, X.; Zhang, S.; Jia, Y.; Feng, S.; Lu, K.; Zhao, J.; Zhang, J.; et al. Superconductivity above 200 K discovered in superhydrides of calcium. *Nat. Commun.* **2022**, *13*, 2863. [[CrossRef](#)]
18. Flores-Livas, J.A.; Boeri, L.; Sanna, A.; Profeta, G.; Arita, R.; Eremets, M. A perspective on conventional high-temperature superconductors at high pressure: Methods and materials. *Phys. Rep.* **2020**, *856*, 1–78. [[CrossRef](#)]
19. Boeri, L.; Hennig, R.; Hirschfeld, P.; Profeta, G.; Sanna, A.; Zurek, E.; Pickett, W.E.; Amsler, M.; Dias, R.; Eremets, M.I.; et al. The 2021 room-temperature superconductivity roadmap. *J. Phys. Condens. Matter* **2022**, *34*, 183002. [[CrossRef](#)]
20. Troyan, I.A.; Semenok, D.V.; Ivanova, A.G.; Kvashnin, A.G.; Zhou, D.; Sadakov, A.V.; Sobolevskiy, O.A.; Pudalov, V.M.; Lyubutin, I.S.; Oganov, A.R. High-temperature superconductivity in hydrides. *Phys. Uspekhi* **2022**, *65*, 748–761. [[CrossRef](#)]
21. Satterthwaite, C.B.; Toepke, I.L. Superconductivity of hydrides and deuterides of thorium. *Phys. Rev. Lett.* **1970**, *25*, 741–743. [[CrossRef](#)]
22. Wittig, J.; Matthias, B.T. Superconducting phosphorus. *Science* **1968**, *160*, 994–995. [[CrossRef](#)] [[PubMed](#)]
23. Eliashberg, G.M. Interactions between electrons and lattice vibrations in a superconductor. *Sov. Phys. JETP* **1960**, *11*, 696–702.
24. Hou, P.; Belli, F.; Bianco, R.; Errea, I. Strong anharmonic and quantum effects in *Pm3n*-AlH₃ under high pressure: A first-principles study. *Phys. Rev. B* **2021**, *103*, 134305. [[CrossRef](#)]
25. Goncharenko, I.; Eremets, M.I.; Hanfland, M.; Tse, J.S.; Amboage, M.; Yao, Y.; Trojan, I.A. Pressure-induced hydrogen-dominant metallic state in aluminum hydride. *Phys. Rev. Lett.* **2008**, *100*, 045504. [[CrossRef](#)]
26. Feng, J.; Grochala, W.; Jaroń, T.; Hoffmann, R.; Bergara, A.; Ashcroft, N.W. Structures and potential superconductivity in SiH₄ at high pressure: En route to “metallic hydrogen”. *Phys. Rev. Lett.* **2006**, *96*, 017006. [[CrossRef](#)]
27. Eremets, M.I.; Trojan, I.A.; Medvedev, S.A.; Tse, J.S.; Yao, Y. Superconductivity in hydrogen dominant materials: Silane. *Science* **2008**, *319*, 1506–1509. [[CrossRef](#)]
28. Li, Y.; Hao, J.; Liu, H.; Li, Y.; Ma, Y. The metallization and superconductivity of dense hydrogen sulfide. *J. Chem. Phys.* **2014**, *140*, 174712. [[CrossRef](#)]
29. Duan, D.; Liu, Y.; Tian, F.; Li, D.; Huang, X.; Zhao, Z.; Yu, H.; Liu, B.; Tian, W.; Cui, T. Pressure-induced metallization of dense (H₂S)₂H₂ with high- T_c superconductivity. *Sci. Rep.* **2014**, *4*, 6968. [[CrossRef](#)]
30. Xu, Y.; Tse, J.S.; Oganov, A.R.; Cui, T.; Wang, H.; Ma, Y.; Zou, G. Superconducting high-pressure phase of cesium iodide. *Phys. Rev. B* **2009**, *79*, 144110. [[CrossRef](#)]
31. Eremets, M.I.; Shimizu, K.; Kobayashi, T.C.; Amaya, K. Metallic CsI at pressures of up to 220 gigapascals. *Science* **1998**, *281*, 1333–1335. [[CrossRef](#)] [[PubMed](#)]
32. Knittle, E.; Jeanloz, R. Structural and bonding changes in cesium iodide at high pressures. *Science* **1984**, *223*, 53–56. [[CrossRef](#)] [[PubMed](#)]
33. Makarenko, I.N.; Goncharov, A.F.; Stishov, S.M. Optical absorption of cesium iodide (CsI) at pressure up to 60 GPa. *Phys. Rev. B* **1984**, *29*, 6018–6019. [[CrossRef](#)]
34. Bardeen, J.; Cooper, L.N.; Schrieffer, J.R. Theory of superconductivity. *Phys. Rev.* **1957**, *108*, 1175–1204. [[CrossRef](#)]
35. Bloch, F. Zum elektrischen Widerstandsgesetz bei tiefen Temperaturen. *Z. Phys.* **1930**, *59*, 208–214. [[CrossRef](#)]
36. Grüneisen, E. Die abhängigkeit des elektrischen widerstandes reiner metalle von der temperatur. *Ann. Phys.* **1933**, *408*, 530–540. [[CrossRef](#)]

37. Matsumoto, R.; Song, P.; Adachi, S.; Saito, Y.; Hara, H.; Yamashita, A.; Nakamura, K.; Yamamoto, S.; Tanaka, H.; Irifune, T. Pressure-induced superconductivity in tin sulfide. *Phys. Rev. B* **2019**, *99*, 184502. [[CrossRef](#)]
38. Kudo, K.; Hiiragi, H.; Honda, T.; Fujimura, K.; Idei, H.; Nohara, M. Superconductivity in Mg₂Ir₃Si: A fully ordered Laves phase. *J. Phys. Soc. Jpn.* **2020**, *89*, 013701. [[CrossRef](#)]
39. Susner, M.A.; Bhatia, M.; Sumption, M.D.; Collings, E.W. Electrical resistivity, Debye temperature, and connectivity in heavily doped bulk MgB₂ superconductors. *J. Appl. Phys.* **2009**, *105*, 195901. [[CrossRef](#)]
40. Pyon, S.; Kudo, K.; Matsumura, J.-I.; Ishii, H.; Matsuo, G.; Nohara, M.; Hojo, H.; Oka, K.; Azuma, M.; Garlea, V.O.; et al. Superconductivity in noncentrosymmetric iridium silicide Li₂IrSi₃. *J. Phys. Soc. Jpn.* **2014**, *83*, 093706. [[CrossRef](#)]
41. Talantsev, E.F. Advanced McMillan's equation and its application for the analysis of highly-compressed superconductors. *Supercond. Sci. Technol.* **2020**, *33*, 094009. [[CrossRef](#)]
42. Talantsev, E.F. An approach to identifying unconventional superconductivity in highly compressed superconductors. *Supercond. Sci. Technol.* **2020**, *33*, 124001. [[CrossRef](#)]
43. Talantsev, E.F.; Stolze, K. Resistive transition of hydrogen-rich superconductors. *Supercond. Sci. Technol.* **2021**, *34*, 064001. [[CrossRef](#)]
44. Talantsev, E.F. Comparison of highly-compressed C2/m-SnH₁₂ superhydride with conventional superconductors. *J. Phys. Condens. Matter* **2021**, *33*, 285601. [[CrossRef](#)]
45. Talantsev, E.F. The electron–phonon coupling constant and the Debye temperature in polyhydrides of thorium, hexadeuteride of yttrium, and metallic hydrogen phase III. *J. Appl. Phys.* **2021**, *130*, 195901. [[CrossRef](#)]
46. Talantsev, E.F. Electron–phonon coupling constant and BCS ratios in LaH_{10–y} doped with magnetic rare-earth element. *Supercond. Sci. Technol.* **2022**, *35*, 095008. [[CrossRef](#)]
47. Carbotte, J.P. Properties of boson-exchange superconductors. *Rev. Mod. Phys.* **1990**, *62*, 1027–1157. [[CrossRef](#)]
48. McMillan, W.L. Transition temperature of strong-coupled superconductors. *Phys. Rev.* **1968**, *167*, 331–344. [[CrossRef](#)]
49. Poole, C.P., Jr. Properties of the normal metallic state. In *Handbook of Superconductivity*, 1st ed.; Poole, C.P., Jr., Ed.; Academic Press: New York, NY, USA, 1999; Volume 1, pp. 31–32.
50. Allen, P.B.; Dynes, R.C. Transition temperature of strong-coupled superconductors reanalyzed. *Phys. Rev. B* **1975**, *12*, 905–922. [[CrossRef](#)]
51. Jiang, H.; Bao, J.-K.; Zhai, H.-F.; Tang, Z.-T.; Sun, Y.-L.; Liu, Y.; Wang, Z.-C.; Bai, H.; Xu, Z.-A.; Cao, G.-H. Physical properties and electronic structure of Sr₂Cr₃As₂O₂ containing CrO₂ and Cr₂As₂ square-planar lattices. *Phys. Rev. B* **2015**, *92*, 205107. [[CrossRef](#)]
52. Zhang, C.; Wang, Y.; Wang, D.; Zhang, Y.; Liu, Z.-H.; Feng, Q.-R.; Gan, Z.-Z. Suppression of superconductivity in epitaxial MgB₂ ultrathin films. *J. Appl. Phys.* **2013**, *114*, 023903. [[CrossRef](#)]
53. Talantsev, E.F. Quantifying the charge carrier interaction in metallic twisted graphene superlattices. *Nanomaterials* **2021**, *11*, 1306. [[CrossRef](#)] [[PubMed](#)]
54. Talantsev, E.F. The dominance of non-electron–phonon charge carrier interaction in highly-compressed superhydrides. *Supercond. Sci. Technol.* **2021**, *34*, 115001. [[CrossRef](#)]
55. Talantsev, E.F. Classifying charge carrier interaction in highly compressed elements and silane. *Materials* **2021**, *14*, 4322. [[CrossRef](#)]
56. White, G.K.; Woods, S.B. Electrical and thermal resistivity of the transition elements at low temperatures. *Phil. Trans. R. Soc. Lond. A* **1959**, *251*, 273–302. [[CrossRef](#)]
57. Paker, D.B.; Klabunde, C.E. Temperature dependence of electrical resistivity of vanadium, platinum, and copper. *Phys. Rev. B* **1982**, *26*, 7012–7014. [[CrossRef](#)]
58. Matula, R.A. Electrical resistivity of copper, gold, palladium, and silver. *J. Phys. Chem. Ref. Data* **1979**, *8*, 1147–1298. [[CrossRef](#)]
59. Shang, T.; Amon, A.; Kasinathan, D.; Xie, W.; Bobnar, M.; Chen, Y.; Wang, A.; Shi, M.; Medarde, M.; Yuan, H.Q.; et al. Enhanced T_c and multiband superconductivity in the fully-gapped ReBe₂₂ superconductor. *New J. Phys.* **2019**, *21*, 073034. [[CrossRef](#)]
60. Stolze, K.; Tao, J.; von Rohr, F.O.; Kong, T.; Cava, R.J. Sc–Zr–Nb–Rh–Pd and Sc–Zr–Nb–Ta–Rh–Pd high-entropy alloy superconductors on a CsCl-type lattice. *Chem. Mater.* **2018**, *30*, 906–914. [[CrossRef](#)]
61. Uemura, Y.J.; Luke, G.M.; Sternlieb, B.J.; Brewer, J.H.; Carolan, J.F.; Hardy, W.N.; Kadono, R.; Kempton, J.R.; Kiefl, R.F.; Kreitzman, S.R. Universal correlations between T_c and $\frac{n_s}{m^*}$ (carrier density over effective mass) in high- T_c cuprate. *Phys. Rev. Lett.* **1989**, *62*, 2317–2320. [[CrossRef](#)] [[PubMed](#)]
62. Uemura, Y.J. Condensation, excitation, pairing, and superfluid density in high- T_c superconductors: The magnetic resonance mode as a roton analogue and a possible spin-mediated pairing. *J. Phys. Condens. Matter* **2004**, *16*, S4515–S4540. [[CrossRef](#)]
63. Talantsev, E.F. Classifying superconductivity in compressed H₃S. *Mod. Phys. Lett. B* **2019**, *33*, 1950195. [[CrossRef](#)]
64. Talantsev, E.F.; Maitaira, R.C. Classifying superconductivity in ThH–ThD superhydrides/superdeuterides. *Mater. Res. Express* **2020**, *7*, 016003. [[CrossRef](#)]
65. Helfand, E.; Werthamer, N.R. Temperature and purity dependence of the superconducting critical field, H_{c2} . II. *Phys. Rev.* **1966**, *147*, 288–294. [[CrossRef](#)]
66. Werthamer, N.R.; Helfand, E.; Hohenberg, P.C. Temperature and purity dependence of the superconducting critical field, H_{c2} . III. Electron spin and spin-orbit effects. *Phys. Rev.* **1966**, *147*, 295–302. [[CrossRef](#)]
67. Orlando, T.P.; McNiff, E.J., Jr.; Foner, S.; Beasley, M.R. Critical fields, Pauli paramagnetic limiting, and material parameters of Nb₃Sn and V₃Si. *Phys. Rev. B* **1979**, *19*, 4545–4561. [[CrossRef](#)]

68. Cao, Y.; Fatemi, V.; Fang, S.; Watanabe, K.; Taniguchi, T.; Kaxiras, E.; Jarillo-Herrero, P. Unconventional superconductivity in magic-angle graphene superlattices. *Nat. Cell Biol.* **2018**, *556*, 43–50. [[CrossRef](#)]
69. Talantsev, E.F.; Mataira, R.C.; Crump, W.P. Classifying superconductivity in Moiré graphene superlattices. *Sci. Rep.* **2020**, *10*, 212. [[CrossRef](#)]
70. Suzuki, Y.; Wakamatsu, K.; Ibuka, J.; Oike, H.; Fujii, T.; Miyagawa, K.; Taniguchi, H.; Kanoda, K. Mott-driven BEC-BCS crossover in a doped spin liquid candidate κ -(BEDT-TTF)₄Hg_{2.89}Br₈. *Phys. Rev. X* **2022**, *12*, 011016. [[CrossRef](#)]
71. Migdal, A.B. Interaction between electrons and lattice vibrations in a normal metal. *Sov. Phys. JETP* **1958**, *7*, 996–1001.
72. Born, M.; Oppenheimer, J.R. Zur Quantentheorie der Molekeln [On the Quantum Theory of Molecules]. *Ann. Der Phys.* **1927**, *389*, 457–484. [[CrossRef](#)]
73. Pietronero, L.; Strässler, S.; Grimaldi, C. Nonadiabatic superconductivity. I. Vertex corrections for the electron-phonon interactions. *Phys. Rev. B* **1995**, *52*, 10516–10529. [[CrossRef](#)] [[PubMed](#)]
74. Grimaldi, C.; Pietronero, L.; Strässler, S. Nonadiabatic superconductivity. II. Generalized Eliashberg equations beyond Migdal's theorem. *Phys. Rev. B* **1995**, *52*, 10530–10546. [[CrossRef](#)]
75. Grimaldi, C.; Cappelluti, E.; Pietronero, L. Isotope effect on m^* in high T_c materials due to the breakdown of Migdal's theorem. *Europhys. Lett.* **1998**, *42*, 667–672. [[CrossRef](#)]
76. Cappelluti, E.; Ciuchi, S.; Grimaldi, C.; Pietronero, L.; Strässler, S. High T_c superconductivity in MgB₂ by nonadiabatic pairing. *Phys. Rev. Lett.* **2002**, *88*, 117003. [[CrossRef](#)] [[PubMed](#)]
77. Pietronero, L.; Boeri, L.; Cappelluti, E.; Ortenzi, L. Conventional/unconventional superconductivity in high-pressure hydrides and beyond: Insights from theory and perspectives. *Quantum Stud. Math. Found.* **2018**, *5*, 5–21. [[CrossRef](#)]